Ab Initio/RRKM Study of the Potential Energy Surface of Triplet Ethylene and Product Branching Ratios of the $C(^3P) + CH_4$ Reaction

Gap-Sue Kim,[†] Thanh Lam Nguyen,[†] Alexander M. Mebel,*[,†] Sheng H. Lin,[†] and Minh Tho Nguyen[‡]

Institute of Atomic and Molecular Sciences, Academia Sinica, P.O. Box 23-166, Taipei 10764, Taiwan, and Department of Chemistry, University of Leuven, Celestijnenlaan, 200F, B-3001 Leuven, Belgium

Received: May 20, 2002; In Final Form: December 2, 2002

Calculations of the lowest triplet state potential energy surface for the $C(^3P) + CH_4$ reaction have been performed using the CCSD(T)/6-311+G(3df,2p)//QCISD/6-311G(d,p) method, and the microcanonical RRKM approach has been used to compute rate constants for individual reaction steps and product branching ratios. The results show that the reaction can occur by abstraction and insertion mechanisms. The abstraction pathway producing $CH(^2\Pi) + CH_3(^2A_2'')$ has a barrier of 26.9 kcal/mol relative to the reactants. The insertion leading to the $HC-CH_3(^3A'')$ intermediate via a 12.2 kcal/mol barrier followed by its isomerization to $H_2C-CH_2-(^3A_1)$ (through a 1,2 H shift) and/or by dissociation with an H-atom loss is found to be a more favorable mechanism. At a low excess internal energy originating from the collision energy (12.2 kcal/mol), the sole reaction products are $C_2H_3 + H$, where 90% of them are formed through the fragmentation of $HC-CH_3$ and the rest (10%) are produced via the H_2C-CH_2 intermediate. At the higher excess internal energy (2 eV), $CH + CH_3$ can be formed mainly through the H-abstraction channel. The calculated $C_2H_3 + H$ and $CH + CH_3$ branching ratios at the excess internal energy of 2 eV are 69.8 and 30.2%, respectively. With further increases of the excess internal energy, the abstraction channel becomes more important, and the $CH + CH_3$ branching ratio increases to 68.9 and 82.8% at 3 and 4 eV, respectively. The $C_2H_2 + H_2$ products can be formed only through the secondary $C_2H_3 + H$ hydrogen disproportionation reactions or via singlet−triplet intersystem crossing in the vicinity of the $HC-CH_3$ intermediate followed by fragmentation of the vibrationally hot ground-state singlet C_2H_4 molecule. Since only the $CH + CH_3$ products have been characterized so far experimentally,[9] new experimental measurements are encouraged.

1. Introduction

Atomic carbon is one of the smallest elements that participates in abstraction, addition, and insertion reactions, which play an important role in combustion, chemical vapor deposition, and interstellar and synthetic hydrocarbon chemistry.[1−3] In the ground electronic triplet state, $C(^3P)$ readily reacts with unsaturated hydrocarbons by a barrierless addition to their double or triple C−C bonds.[4] However, triplet carbon atoms are much less reactive with respect to saturated species. For example, although the reaction of the electronically excited $C(^1D)$ atom with molecular hydrogen is very fast[5] and proceeds by insertion into the H−H bond along the C_{2v}-symmetric vertical minimum-energy pathway without a barrier,[6] for the triplet atomic carbon, this path is symmetry-forbidden,[6] and the $C(^3P) + H_2$ reaction can take place only at high available energies. Hyperthermal triplet carbon atoms do react with saturated molecules, and two primary reaction mechanisms have been proposed—an insertion into a σ bond and hydrogen abstraction.[7] Recent experimental studies have examined the reaction dynamics of the $C(^3P)$ atoms, which were generated by laser ablation of graphite and possessed an energy of 2 eV and higher, with H_2, HCl, HBr, CH_3OH,[8] and CH_4.[9] The crossed molecular beam technique was employed, and the CH product was probed via laser-induced fluorescence. On the basis of theoretical investigations[10,11] and comparisons of the CH rotational distributions with those from the reactions of $C(^1D)$ with H_2 and HCl,[12] the reactions of $C(^3P)$ were suggested to proceed via an insertion mechanism involving carbene intermediates.[8,9] This mechanism was also supported by the trajectory calculations for the $C(^3P) + H_2$ reaction,[13] which generated CH internal distributions in agreement with the experimental observations. However, the analogy between the $C(^3P) + CH_4$ and $C(^3P) + H_2$ reactions used for interpreting the experimental data in ref 9 may not be warranted since the C_2H_4 potential energy surface (PES) is more complex than that for CH_2 and the $C(^3P) + CH_4$ reaction may lead to a larger variety of products, including $C_2H_3 + H$, $C_2H_2 + H_2$, and $CH_2 + CH_2$ in addition to $CH + CH_3$.

Although the PES and reaction dynamics for the prototype $C(^3P) + H_2$ reaction have been investigated theoretically in a great detail,[6,13] much less is known about the $C(^3P) + CH_4$ reaction. The structures of the triplet $HC-CH_3$ and H_2C-CH_2 intermediates are well established, and the former was calculated to lie ∼5.2 kcal/mol higher in energy than the latter.[14,15] However, studies of the reaction PES were limited to relatively low-level MP4/6-31G(d,p)//HF/6-31G(d) calculations by Sakai et al.,[16] who calculated the initial reaction barrier to be 30.6 kcal/mol. The authors labeled the reaction mechanism as "near abstraction", but in the absence of intrinsic reaction coordinate (IRC) calculations, it was not clear whether the transition state they found corresponds to the insertion or abstraction process. In the present paper, we report the results of detailed high-level

* Corresponding author. E-mail: mebel@po.iams.sinica.edu.tw.
† Academia Sinica.
‡ University of Leuven.

10.1021/jp0261410 CCC: $25.00
Published on Web 02/20/2003

ab intio calculations of PES for the $C(^3P) + CH_4$ reaction, which provide accurate energies of intermediates and transition states and give insight into the reaction mechanism. The calculated molecular parameters and energetics are then used for RRKM calculations of rate constants for individual reaction steps and relative yields (branching ratios) of the products at various excess internal energies, and the results are compared with available experimental data.

2. Computational Details

2.1. Ab Initio Calculations of PES. Various intermediates and transitions states on the lowest triplet state PES of the reaction of $C(^3P)$ with CH_4 have been optimized using the QCISD method[17] with the 6-311G(d,p) basis set. Vibrational frequencies have also been calculated at the QCISD/6-311G-(d,p) level for the characterization of stationary points (number of imaginary frequencies NIMAG = 0 and 1 for local minima and transition states, respectively) and to obtain zero-point energy (ZPE) corrections. The energies were then refined by single-point coupled-cluster[18] CCSD(T)/6-311+G(3df,2p) calculations so that the overall theoretical level can be written as CCSD(T)/6-311+G(3df,2p)//QCISD/6-311G(d,p) + ZPE[QCISD/6-311G(d,p)].

For the transition states, we additionally performed geometry optimization using the HF, MP2,[19] hybrid density functional B3LYP,[20] and multireference complete active space self-consistent field (CASSCF)[21] methods with the 6-311G(d,p) or 6-311+G(d,p) basis sets. The active space in CASSCF calculations included 10 electrons distributed on 10 orbitals. For instance, we located the abstraction transition state TS2 at the HF/6-311G(d,p) and CASSCF(10,10)/6-311+G(d,p) levels of theory. To obtain a more accurate relative energy of this transition state, we carried out internally contracted multireference configuration interaction (MRCI)[22] calculations with the correlation-consistent aug-cc-pVTZ basis set,[23] MRCI+Q-(10,10)/aug-cc-pVTZ//CASSCF(10,10)/6-311+G(d,p). The active space used for MRCI was the same as that for CASSCF, and wave functions from CASSCF were employed as references in the MRCI calculations. All calculations were carried out using the MOLPRO 98[24] and Gaussian 98[25] programs.

2.2. Rate-Constant Calculations Using the RRKM Theory. For a unimolecular reaction

$$A^* \xrightarrow{k} A^{\ddagger} \rightarrow P$$

where A* is the energized reacant, $A^{\ddagger}$ is the activated complex or transition state on the PES, and P represents the product or products, the microcanonical rate constant $k(E)$ at an available energy E can be expressed by the quasi-equilibrium theory or RRKM theory as follows:[26]

$$k(E) = \frac{\sigma}{h}\frac{W^{\ddagger}(E - E^{\ddagger})}{\rho(E)}$$

σ is the reaction-path degeneracy, h is the Planck constant, and $E^{\ddagger}$ is the adiabatic barrier height. $W^{\ddagger}(E - E^{\ddagger})$ denotes the number of accessible internal (vibrational) states of the transition state (i.e., the vibrational states with energies between 0 and $E - E^{\ddagger}$), and $\rho(E)$ shows the density of states of the energized reactant molecule. The direct count, saddle-point, or Whitten−Rabinovitch methods[26−28] can be used to calculate the $W^{\ddagger}(E - E^{\ddagger})$ and $\rho(E)$ values. For the $HC-CH_3(^3A'') \rightarrow CH(^2\Pi) + CH_3(^2A_2'')$ decomposition channel, which does not exhibit an exit barrier on the PES, the microcanonical variational state theory (MVTST)[28] was employed. The variational transition-state position was located on the basis of the following criterion:

$$\frac{\partial k(E)}{\partial R_c} = 0 \quad \text{or} \quad \frac{\partial W(E, R_c)}{\partial R_c} = 0$$

where W is the number of states and R_c is the reaction coordinate, which is the length of the breaking C−C for the aforementioned reaction. In the calculations of the number and density of states, we used QCISD/6-311G(d,p) frequencies scaled by 0.9776[29] to account for their anharmonicity for $0 \rightarrow 1$ transitions. Otherwise, the harmonic approximation was employed to calculate the total number and density of states. For the case in which the excitation energy is large and there exist low-frequency modes, the harmonic approximation will not be accurate for low-frequency modes in calculating the total number and density of states and may introduce certain errors into our treatment. More sophisticated RRKM calculations are required in this case, but they are beyond the scope of the present work.

We carried out the RRKM calculations for two values of the internal energy in excess of the reactants' zero-point level, corresponding to the collision energies of 12.2 kcal/mol (the minimal energy needed to overcome the barrier for the insertion channel) and 46.1 kcal/mol (corresponding to the collision energy of 2 eV used in the experiment[9]). One part of the collision energy in a molecular beam experiment goes to the vibrational (internal) energy of the complex formed, and another part ends up as overall rotational energy. Therefore, to achieve a certain value of the excess internal energy, higher collision energy is required. The calculations were performed for zero-pressure conditions because no energy transfer occurs in crossed molecular beam experiments.

2.3. Rate Equations and Branching Ratios. Under collision-free conditions, the master equations for a unimolecular reaction can be expressed as follows:

$$\frac{d[C]_i}{dt} = \sum k_n[C]_j - \sum k_m[C]_i$$

where $[C]_i$ and $[C]_j$ are the concentrations of various intermediates or products and k_n and k_m are microcanonical constants calculated using the RRKM theory. The fourth-order Runge−Kutta method[28] was employed to solve the master equations and to obtain numerical solutions for the concentrations of various products versus time. The concentrations at the times when they have converged were used for calculations of the product branching ratios.

3. Results and Discussion

Total energies, zero-point vibrational energies (ZPE), and relative energies for various species computed at the QCISD/6-311G(d,p) and CCSD(T)/6-311+G(3df,2p) levels of theory are given in Table 1. Vibrational frequencies calculated at the QCISD/6-311G(d,p) and other theoretical levels are presented in Table 2. The rate constants for individual reaction steps obtained using the RRKM theory are listed in Table 3. Optimized geometries of various local minima and transition states calculated at different levels of theory are shown in Figure 1. The profile of the PES for the $C(^3P) + CH_4$ reaction is presented in Figure 2. The reaction scheme for kinetic calculations was built upon the PES, and for the reaction-rate coefficients, we used the same numbering as for corresponding transition states.

TABLE 1: Total Energies (in hartrees), Zero-Point Energies (ZPE, in kcal/mol), and Relative Energies (in kcal/mol) of Various Species Calculated at the QCISD/6-311G(d,p) and CCSD(T)/6-311+G(3df,2p) Levels of Theory

	total energy			relative energy	
species	QCISD/ 6-311G(d,p)	CCSD(T)/ 6-311+G(3df,2p)	ZPE	QCISD/ 6-311G(d,p)	CCSD(T)/ 6-311+G(3df,2p)
$C(^3P) + CH_4(T_d-{}^1A_1)$	−78.16724	−78.21208	28.32	0.0	0.0
$CH(C_{\infty v}-{}^2\Pi) + CH_3(D_{3h}-{}^2A_2'')$	−78.11665	−78.16545	22.73	26.3	23.8
$C_2H_3(C_s-{}^2A') + H(^2S)$	−78.19160	−78.24810	23.12	−20.4	−27.7
$HCCH(C_{2v}-{}^3B_2) + H_2(D_{\infty h}-{}^1\Sigma^+_g)$	−78.16021	−78.21519	21.55	−2.2	−8.6
$H_2CC(C_{2v}-{}^3B_2) + H_2(D_{\infty h}-{}^1\Sigma^+_g)$	−78.15946	−78.21189	22.10	−1.2	−6.0
$2CH_2(C_{2v}-{}^3B_1)$	−78.10523	−78.15020	21.89	32.6	32.5
$H_2C-CH_2(D_{2d}-{}^3A_1)$	−78.27059	−78.32536	28.66	−64.5	−70.8
$HC-CH_3(C_s-{}^3A'')$	−78.26564	−78.31830	30.05	−60.0	−65.0
$C-CH_4(C_{3v}-{}^3E)$	−78.16822	−78.21357	28.51	−0.4	−0.8
$TS1(C_s-{}^3A'')$	−78.13282	−78.18985	26.48	19.8	12.2
$TS2(C_{3v}-{}^3E)$			23.01[a]		26.9[b]
$TS3(C_1-{}^3A)$	−78.18455	−78.24263	26.34	−12.8	−21.1
$TS4(C_1-{}^3A)$	−78.18828	−78.24545	24.13	−17.3	−25.0
$TS5(C_1-{}^3A)$	−78.18334	−78.24207	24.27	−14.1	−22.8
$TS6(C_s-{}^3A')$	−78.15023	−78.20626	22.35	4.8	−2.2
$TS7(C_s-{}^3A')$	−78.14977	−78.20722	22.21	5.0	−2.9

[a] Calculated at the CASSCF(10,10)/6-311+G(d,p) level. [b] The number is derived from the relative energy of TS2 (97.7 kcal/mol) with respect to that of $H_2C-CH_2(D_{2d},{}^3A_1)$ calculated at the MRCI+Q(10,10)/aug-cc-pVTZ//CASSCF(10,10)/6-311+G(d,p) level of theory with the CASSCF(10,10)/6-311+G(d,p) ZPE.

TABLE 2: Vibrational Frequencies (in cm^{-1}, Scaled by 0.9776) of Various Species Calculated at the QCISD/6-311G(d,p) Level[a]

H_2C-CH_2 ($D_{2d}-{}^3A_1$)	$HC-CH_3$ ($C_s-{}^3A''$)	$C-CH_4$ ($C_{3v}-{}^3E$)	TS1 ($C_s-{}^3A''$)	TS2 ($C_{3v}-{}^3E$)[b]	TS3 ($C_1-{}^3A$)	TS4 ($C_1-{}^3A$)	TS5 ($C_1-{}^3A$)	TS6 ($C_s-{}^3A'$)	TS7 ($C_s-{}^3A'$)
339.4	200.7	44.4	935.1i	1712.0i	2170.0i	647.8i	1003.7i	812.9i	971.6i
339.8	768.6	44.4	159.7	120.2	340.6	329.8	393.7	141.0	182.4
662.2	992.0	75.5	633.3	337.6	745.5	427.9	496.9	155.0	340.3
925.6	1066.6	1336.9	777.4	445.1	797.9	725.0	711.1	632.8	782.7
925.6	1105.3	1336.9	892.0	881.6	984.8	805.1	832.2	645.9	802.6
1109.6	1383.6	1337.0	1222.9	973.3	1085.6	912.6	885.2	830.2	804.6
1424.3	1450.9	1535.3	1397.4	991.8	1205.3	1063.8	1039.8	979.5	926.2
1449.0	1456.4	1535.3	1436.2	1222.8	1397.1	1355.1	1361.6	1383.3	1075.8
3060.6	2938.8	2976.0	2462.0	1298.3	2175.5	1524.4	1525.5	1546.2	1627.3
3062.7	2991.8	3090.6	2962.9	2665.9	3039.3	3036.6	3031.1	2871.9	2534.7
3150.0	3038.4	3090.6	3068.1	2756.3	3100.0	3136.5	3131.8	3011.5	3026.4
3150.0	3159.3	3095.5	3096.6	2793.5	3142.1	3186.9	3189.2	3086.4	3084.3

[a] Unless otherwise mentioned. [b] Calculated at the CASSCF(10,10)/6-311+G(d,p) level and scaled by 0.9.

TABLE 3: Calculated Microcanonical Rate Constants (in s^{-1}) for Various Reaction Channels

	excess internal energy					
	12.2 kcal/mol			46.1 kcal/mol (2 eV)		
rate constant	(1)	(2)	(3)	(1)	(2)	(3)
k_1	2.62×10^8	1.84×10^8	3.78×10^5	4.10×10^{10}	4.19×10^{10}	4.17×10^{10}
k_{-1}	3.21×10^5	3.20×10^5	3.22×10^5	6.39×10^9	6.44×10^9	6.40×10^9
k_2	0.0	0.0	0.0	1.71×10^{10}	1.76×10^{10}	1.74×10^{10}
k_3	1.89×10^{11}	1.91×10^{11}	1.89×10^{11}	1.65×10^{12}	1.66×10^{12}	1.66×10^{12}
k_{-3}	4.96×10^{10}	5.01×10^{10}	4.98×10^{10}	4.87×10^{11}	4.89×10^{11}	4.89×10^{11}
k_4	1.31×10^{12}	1.31×10^{12}	1.31×10^{12}	9.75×10^{12}	9.76×10^{12}	9.75×10^{12}
k_5	1.70×10^{11}	1.72×10^{11}	1.71×10^{11}	1.67×10^{12}	1.67×10^{12}	1.67×10^{12}
k_{var}	0.0	0.0	0.0	2.23×10^{10}	2.24×10^{10}	2.23×10^{10}

(1) Direct count method. (2) Saddle-point method. (3) Whitten−Rabinovitch method.

At the initial reaction stage, the $C(^3P)$ atom can form a weak van der Waals complex with the CH_4 molecule stabilized by 0.8 kcal/mol with respect to the reactants. The $C-CH_4$ complex has C_{3v} symmetry and a ^3E electronic state, and the attacking carbon atom is located on a 3-fold axis of the methane molecule. C and CH_4 are still far from each other in the complex, with C−C and C−H distances of 3.23 and 3.05 Å, respectively. After the weakly bound $C-CH_4$ intermediate is formed, the reaction can proceed by the direct hydrogen abstraction mechanism, or the carbon atom can insert into a C−H bond.

3.1. Hydrogen Abstraction Mechanism. Starting from the $C-CH_4$ complex, the attacking carbon atom can continue to approach one of methane's hydrogen atoms so that the corresponding C−H bond elongates and a new C−H bond begins to form. During this process, the methane molecule rotates around the line perpendicular to the C_3 axis in a symmetry plane toward the approaching carbon atom, and the symmetry of the system is reduced from C_{3v} to C_s. When the abstraction transition state TS2 is reached, the symmetry of the molecule again becomes C_{3v}, but the order of the atoms on the 3-fold axis in the transition state is C−H−C instead of H−C−C in the initial complex. After clearing the transition state, the CH and CH_3 fragments depart from each other. We were able to locate TS2 at the CASSCF-(10,10)/6-311+G(d,p) level, but the abstraction TS search using

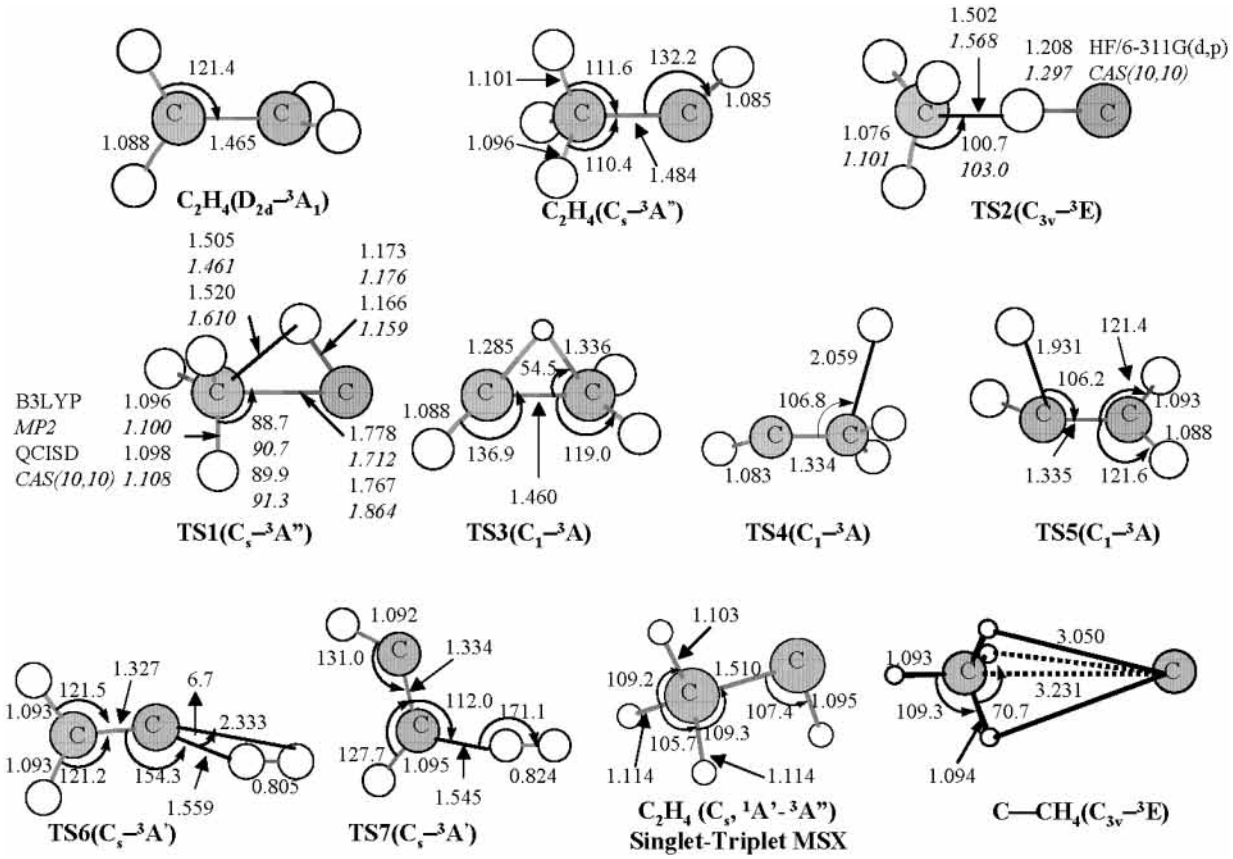

Figure 1. Optimized geometries of various local minima and transition states in the $C(^3P) + CH_4$ reaction calculated at the QCISD/6-311G(d,p) level (unless otherwise mentioned) and other levels of theory. (Bond lengths are given in angstroms, and bond angles, in degrees).

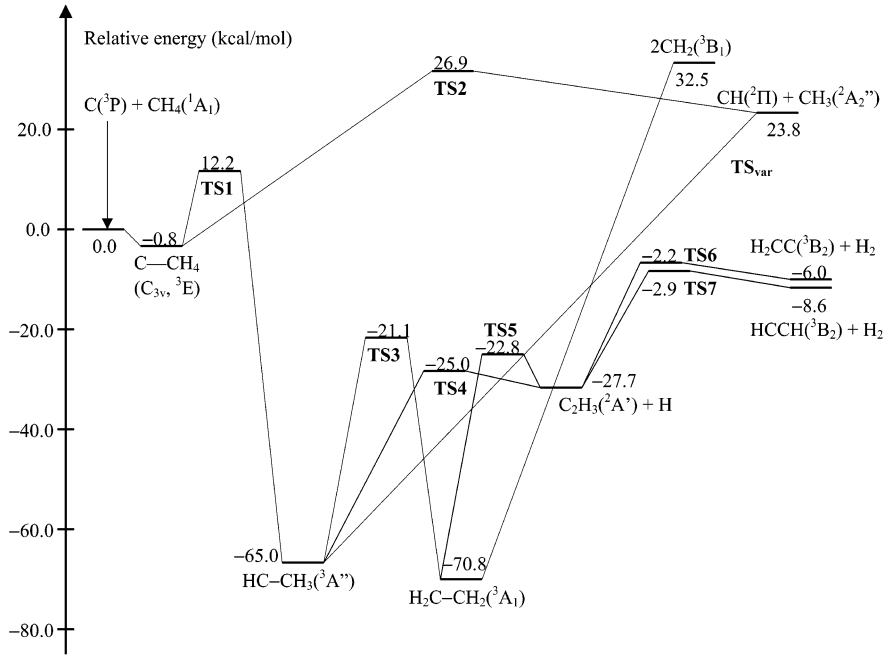

Figure 2. Calculated profile of the potential energy surface for the $C(^3P) + CH_4$ reaction.

single-reference methods [except HF/6-311G(d,p)] did not succeed. According to its geometry, TS2 has late character, with breaking and forming C−H bond lengths of 1.57 and 1.30 Å, respectively. This result is in accord with the reaction endothermicity; the calculated heat of the $C(^3P) + CH_4(^1A_1) \rightarrow CH(^2\Pi) + CH_3(^2A_2'')$ reaction is 23.8 kcal/mol, close to the experimental value of 23.4 kcal/mol.[30] At the MRCI+Q(10,10)/aug-cc-pVTZ//CASSCF(10,10)/6-311+G(d,p) level with ZPE obtained by the CASSCF(10,10)/6-311+G(d,p) calculations, TS2 lies 97.7 kcal/mol above the $H_2C-CH_2(^3A_1)$ intermediate, which gives its relative energy with respect to $C(^3P) + CH_4(^1A_1)$ as 26.9 kcal/mol (Table 1). The barrier for the reverse $CH(^2\Pi) + CH_3(^2A_2'') \rightarrow C(^3P) + CH_4(^1A_1)$ hydrogen abstraction reaction is only 3.1 kcal/mol.

The near abstraction barrier obtained by Sakai et al.,[16] 30.6 kcal/mol at the MP4/6-31G(d,p)//HF/6-31G(d) level, is rather

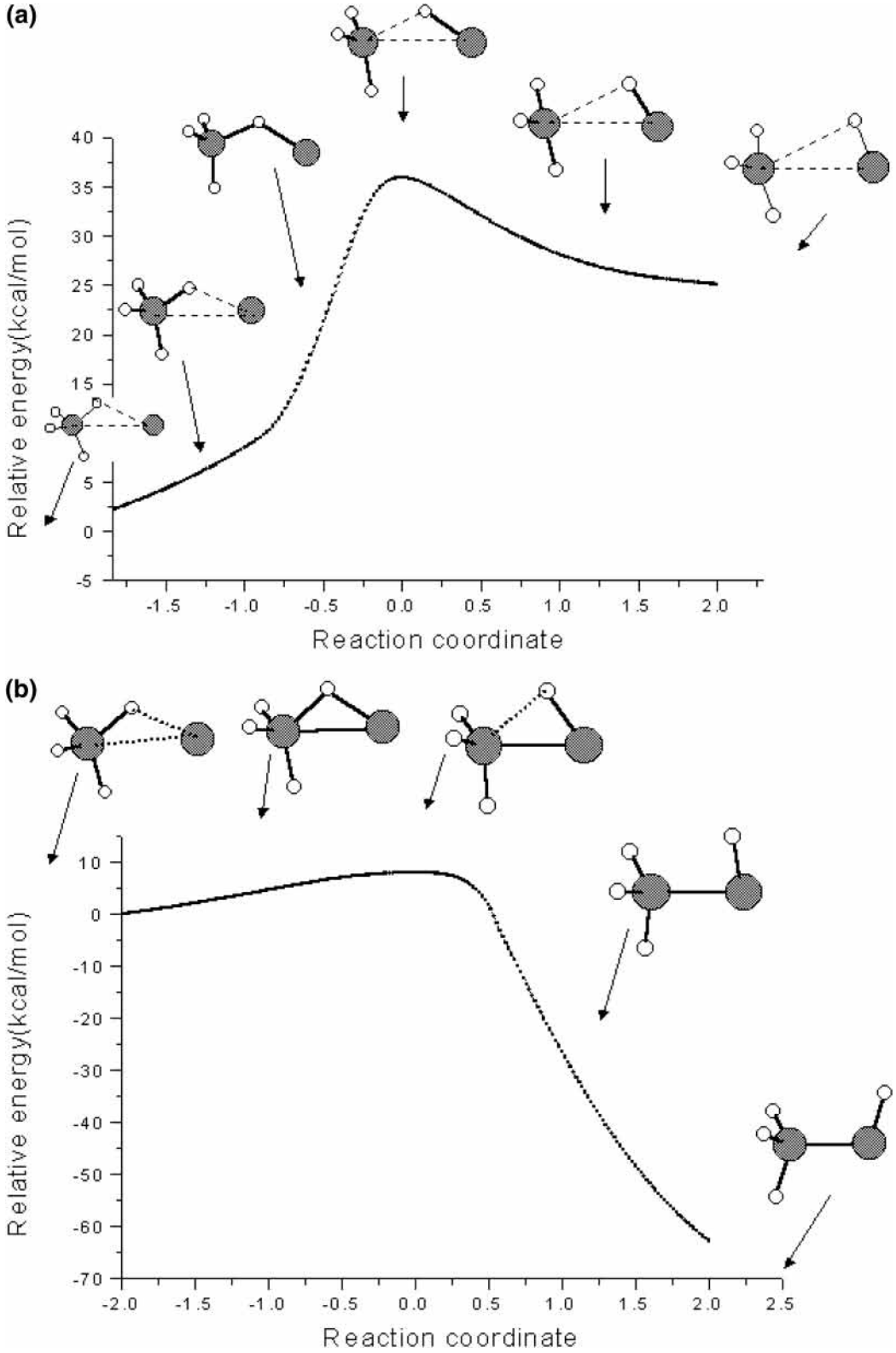

Figure 3. Profiles of the minimum-energy reaction pathways obtained from IRC calculations (a) for the near abstraction transition state from ref 16, calculated at the UHF/6-31G(d) level and (b) for the insertion transition state TS1 calculated at the B3LYP/6-311G(d,p) level.

close to the abstraction barrier of 26.9 kcal/mol obtained by us. To clarify the nature of the transition state reported by Sakai et al., we calculated the intrinsic reaction coordinate (IRC)[31] using their HF/6-31G(d) approximation. The calculated profile of PES along with the structures of some intermediate points on the minimum-energy reaction path is shown in Figure 3a. As one can see, the transition state corresponds to the hydrogen abstraction process. However, the HF/6-31G(d) optimized geometry of the abstraction TS is rather different from that of TS2 obtained at the CASSCF(10,10)/6-311+G(d,p) level, which possesses C_{3v} symmetry. Thus, the HF/6-31G(d) approach is apparently not able to reproduce the correct geometry of the abstraction TS, although the MP4/6-31G(d,p)//HF/6-31G(d) barrier height is not far from our MRCI value.

3.2. Insertion Mechanism. According to our CCSD(T)/6-311+G(3df,2p)//QCISD/6-311G(d,p) calculations, the insertion

mechanism of the $C(^3P) + CH_4$ reaction in the lowest triplet electronic state generates an intermediate $HC-CH_3(^3A'')$ via transition state TS1 with barriers of 13.0 and 12.2 kcal/mol relative to the $C-CH_4$ complex and the initial reactants, respectively. Again, along the reaction pathway from $C-CH_4$ to TS1, the methane molecule turns in the direction of the attacking carbon atom, and the symmetry decreases from C_{3v} to C_s. In the transition state, the breaking C−H bond length increases to 1.52 Å (at the QCISD/6-311G(d,p) level), and two new bonds start to form, C−C (1.77 Å) and C−H (1.17 Å). After TS1, the attacked hydrogen atom continues to move away from the methane's carbon while the attacking C approaches its methane counterpart, thus completing the formation of the C−C and C−H bonds. As seen in Figure 1, different methods gave quite similar geometric parameters for TS1, and the results of B3LYP/6-311G(d,p) and QCISD/6-311G(d,p) calculations are especially close. The CASSCF(10,10)-optimized C−C and breaking C−H bond lengths are about 0.1 Å longer than those obtained at the B3LYP and QCISD levels. The nature of TS1 has been confirmed by IRC calculations at the B3LYP/6-311G-(d,p) level. As seen in Figure 3b, TS1 clearly connects the reactants with the $HC-CH_3$ product (i.e., it is an insertion transition state).

The insertion barrier is 14.7 kcal/mol lower than the abstraction barrier at TS2, so the insertion mechanism is clearly preferable as compared to the direct hydrogen abstraction. This result is in agreement with the experimental observations by Scholefield et al.,[9] who concluded that the $C(^3P) + CH_4$ reaction proceeds by the insertion mechanism via a triplet $HC-CH_3$ intermediate. Similar behavior was reported earlier for the $C(^3P) + H_2 \rightarrow CH + H$ reaction,[11] where H abstraction through a collinear $C_{\infty v}$ path along the $^3\Pi$ surface has a high barrier but the reaction via the insertion mechanism can proceed with no barrier. The barrier is lowered because of the interaction of the empty p orbital of the $C(^3P)$ pointing toward H_2 with the occupied orbital of the hydrogen molecule. The importance of an empty orbital of the reactant in directing reactivity at long range has also been recognized in other insertion reactions, for instance, those of carbene with hydrocarbons.[1,32] Apparently, the attractive long-range interaction between the empty p orbital of the carbon atom and the highest occupied molecular orbital (HOMO) of CH_4 makes the insertion mechanism predominant for the $C(^3P)$ reaction methane.

$HC-CH_3$ has C_s symmetry and a $^3A''$ electronic state, and its relative energy with respect to the reactants, −65.0 kcal/mol at the CCSD(T)//6-311+G(3df,2p)//QCISD/6-311G(d,p) level, is close to the value of −61.5 kcal/mol obtained by Sakai et al. in their MP4/6-31G(d,p)//HF/6-31G(d) calculations.[16] The $HC-CH_3$ intermediate can rearrange by the 1,2 hydrogen migration via TS3, leading to the other isomer of triplet C_2H_4, D_{2d}-symmetric $H_2C-CH_2(^3A_1)$, which lies 5.8 kcal/mol lower in energy than $HC-CH_3(^3A'')$ and 70.8 kcal/mol below the reactants. The H-shift transition state TS3, which lies 21.1 kcal/mol lower in energy than the initial reactants, has no symmetry, and the barrier heights for the forward and reverse reactions are 43.9 and 49.7 kcal/mol, respectively.

There exist two decomposition pathways of $HC-CH_3(^3A'')$ leading to the $C_2H_3(^2A') + H$ and $CH(^2\Pi) + CH_3(^2A_2'')$ products. The hydrogen-elimination channel occurs via a nonsymmetric transition state TS4 via a barrier of 40.0 kcal/mol. The reverse barrier for the H-atom addition to the CH_2 group in C_2H_3 on the triplet PES is as low as 2.7 kcal/mol. TS4 is a productlike transition state with a C−H separation of 2.06 Å for the breaking bond. The overall calculated exothermicity for the $C(^3P) + CH_4 \rightarrow C_2H_3(^2A') + H$ reaction is 27.7 kcal/mol, in reasonably good agreement with the experimental value of 30.3 kcal/mol.[30] This reaction channel is the most favorable energetically if one considers only spin-allowed product channels. A cleavage of the C−C bond gives the $CH(^2\Pi) + CH_3(^2A_2'')$ products without an exit barrier. This process is highly endothermic since the calculated C−C bond strength in the triplet carbene $HC-CH_3(^3A'')$ is 88.8 kcal/mol. The energy-dependent variational transition states for this channel were obtained using the microcanonical variational transition-state theory.

For the other triplet C_2H_4 isomer, $H_2C-CH_2(^3A_1)$, two decomposition pathways that generate the $C_2H_3(^2A') + H$ and $2CH_2(^3B_1)$ products are possible. The $H_2C-CH_2 \rightarrow C_2H_3(^2A') + H$ channel takes place through TS5 by an H-atom loss. TS5 has no symmetry and, similar to TS4, is a late transition state where the breaking C−H bond is elongated to 1.93 Å. The calculated barrier height for the H-elimination pathway is 48.0 kcal/mol. Interestingly, the reverse barrier for the H addition to the CH group of the vinyl radical on the triplet PES, 4.9 kcal/mol, is higher than that for the H addition to the CH_2 group, 2.7 kcal/mol at TS4. Alternatively, if a subsequent reaction of C_2H_3 with H could occur, this would much more likely proceed on the singlet PES, where the recombination is barrier-free. The C−C bond cleavage in the H_2C-CH_2 intermediate yielding two triplet carbene biradicals, $2CH_3(^3B_1)$, takes place without an exit barrier. However, this process is highly endothermic, by 103.3 kcal/mol, and is not likely to contribute to the reaction.

We have also tried to locate transition states for molecular hydrogen elimination from the $HC-CH_3$ and H_2C-CH_2 intermediates. Various attempts to locate saddle points for these processes converged to transition states TS6 and TS7. However, IRC calculations showed that TS6 and TS7 are not H_2 elimination/addition transition states but rather H-atom abstraction/disproportionation transition states. For instance, TS6 corresponds to the $C_2H_3 + H \rightarrow H_2CC(^3B_2) + H_2$ reaction, and TS7 connects $C_2H_3 + H$ with $HCCH(^3B_2) + H_2$. Indeed, TS6 and TS7, which both have C_s symmetry and $^3A'$ electronic states, depict geometric structures that are typical of the H-abstraction transition states with nearly linear C−H−H fragments. The calculated barriers with respect to $C_2H_3 + H$ are 25.5 and 24.8 kcal/mol, respectively, whereas the barriers for the reverse $H_2CC(^3B_2) + H_2 \rightarrow C_2H_3 + H$ and $HCCH(^3B_2) + H_2 \rightarrow C_2H_3 + H$ reactions are relatively low, 3.8 and 5.7 kcal/mol. Thus, our results indicate that direct H_2 loss from the triplet C_2H_4 species is not possible. The $C_2H_2 + H_2$ products on the triplet PES can be formed only through secondary reactions of the vinyl radical with H atoms. Therefore, under single-collision conditions, H_2 is not expected to be a product of the $C(^3P) + CH_4$ reaction occurring on the triplet PES. Triplet H_2CC and HCCH species are in a sense isoelectronic to the doublet H_2CCH radical where one of the C−H bonds is replaced by an unpaired electron. Earlier,[33] we established that the H_2 addition to the vinyl radical to produce C_2H_5 is also not possible; the $C_2H_3 + H_2$ reaction rather proceeds by H abstraction, producing $C_2H_4 + H$. The reason for this preference can be rationalized in terms of the molecular orbital picture. To break the H−H bond in molecular hydrogen, electron density has to be donated from the singly occupied orbital of C_2H_3 or triplet C_2H_2 to the σ_u antibonding orbital of H_2. The singly occupied orbital is located in the molecular plane and has mostly p character. If H_2 approaches C_2H_3 or triplet C_2H_2 perpendicularly to this plane, its σ_u orbital cannot interact with the singly occupied p orbital of the attacked radical (or biradical). The maximal interaction

is achieved when H_2 approaches C_2H_3 or triplet C_2H_2 in the molecular plane and parallel to the singly occupied p orbital. Such an approach results in a nearly linear C−H−H arrangement in the transition state, and the reaction proceeds by H abstraction instead of H_2 addition. A similar situation is also found for other reactions of σ radicals with H_2, for instance, $C_2H + H_2 \rightarrow C_2H_2 + H$[34] and $HCCCC + H_2 \rightarrow HCCCCH + H$,[35] and we believe this is a common feature of the σ radicals.

Summarizing the calculated PES of the insertion mechanism for the $C(^3P) + CH_4(^1A_1)$ reaction, the $HC-CH_3(^3A'') \rightarrow$ TS4 $\rightarrow C_2H_3(^2A') + H$ and $HC-CH_3(^3A'') \rightarrow$ TS3 $\rightarrow H_2C-CH_2(^3A_1) \rightarrow$ TS5 $\rightarrow C_2H_3(^2A') + H$ channels are most favorable energetically, and $C_2H_3(^2A') + H$ are believed to be the major products.

3.3. Microcanonical Rate Constants and Product Branching Ratios. The computed microcanonical rate constants are presented in Table 3. We considered two excess internal energies, 12.2 kcal/mol and the experimental value of 46.1 kcal/mol (2 eV).[9] The reason to choose 12.2 kcal/mol as an excess internal energy is that at least this energy is required to overcome the barrier at TS1 (i.e., this is the minimal energy needed for the reaction to occur). In general, the rate constants obtained by the direct count method are in reasonable agreement with those calculated using the Whitten−Rabinovitch approximation and the saddle-point method, except for the rate constant k_1 of the $C-CH_4 \rightarrow$ TS1 $\rightarrow HC-CH_3$ channel with the excess internal energy of 12.2 kcal/mol. In this case, the excess internal energy is equal to the barrier height, and the saddle-point method and especially the Whitten−Rabinovitch approximation greatly underestimate the most accurate direct count value. The number of accessible vibrational states of TS1 was taken as 1 in all three methods, and the error in the Whitten−Rabinovitch approximation arises from calculations of the density of states for the $C-CH_4$ complex, for which the Whitten−Rabinovitch value is 3 orders of magnitude higher than those obtained by the direct count and saddle-point methods. The origin of this error is in the low vibrational frequencies for $C-CH_4$ and its low available internal energy (13 kcal/mol). These factors are not present for $HC-CH_3$ and its densities of states; correspondingly, k_{-1} values computed by the three methods are nearly the same.

We assumed the weakly bound $C-CH_4$ complex to be a reaction intermediate, which may not be the case because of its low binding energy and correspondingly short lifetime. Nevertheless, the cross sections of the $C(^3P) + CH_4 \rightarrow$ TS2 $\rightarrow CH + CH_3$ and $C(^3P) + CH_4 \rightarrow$ TS1 $\rightarrow HC-CH_3$ reactions in the case of RRKM behavior should be proportional to the numbers of states of transition states[26] TS2 and TS1, respectively, just like the RRKM-calculated microcanonical rate constants for the $C-CH_4 \rightarrow$ TS2 $\rightarrow CH + CH_3$ and $C-CH_4 \rightarrow$ TS1 $\rightarrow HC-CH_3$ processes. For instance, the weighted-average cross section $\langle\sigma\rangle$ can be computed as[36,37]

$$\langle\sigma\rangle = \frac{\kappa h^2}{8\pi\mu}\frac{W^{\ddagger}(E-E^{\ddagger})}{W_E(E)}$$

where κ is the transmission coefficient, μ is the reduced mass of the reactants, and $W_E(E)$ is the energy density function

$$W_E(E) = \sum_{ij}(E-\epsilon_{ij})\,H(E-\epsilon_{ij}) = (2\pi i)^{-1}\int_{\gamma-i\infty}^{\gamma+i\infty}\frac{d\beta}{\beta^2}e^{\beta E}Q_{re}^{int}(\beta)$$

where $\beta = 1/kT$, k is the Boltzmann constant, T is the temperature of the reactants, and $Q_{re}^{int}(\beta)$ is the partition function of the reactants. On the basis of this, the relative probabilities of the abstraction and insertion channels can be described by the ratio of rate constants k_1 and k_2, which have a common denominator—the density of states of $C-CH_4$—and a common numbers of states for TS1 and TS2 in their numerators.

At the excess internal energy of 12.2 kcal/mol, the $C-CH_4 \rightarrow CH + CH_3$ and $HC-CH_3 \rightarrow CH + CH_3$ channels are closed, and the corresponding rate constants k_2 and k_{var} are zero. Therefore, $C_2H_3 + H$ is the only reaction product. It is noteworthy that the rate constant k_4 for the $HC-CH_3 \rightarrow H_2C{=}CH + H$ channel, 1.31×10^{12} s^{-1}, is about 7 times faster than k_3 for the $HC-CH_3 \rightarrow H_2C-CH_2$ isomerization, indicating that most of the products are formed by H loss from $HC-CH_3$. Indeed, steady-state calculations give the branching ratio of the $C_2H_3 + H$ products formed from $HC-CH_3$ and H_2C-CH_2 as 90/10. At the excess internal energy of 46.1 kcal/mol, the $CH + CH_3$ product channel opens up and is able to compete with the production of $C_2H_3 + H$. The probability of the abstraction reaction channel related to k_2 is only a factor of 2.4 lower than the probability of the insertion channel (related to k_1) leading initially to the $HC-CH_3$ intermediate. The branching ratios of the $C_2H_3 + H$ and $CH + CH_3$ products are computed as 69.8 and 30.2%. Most of the $CH + CH_3$ products (99.5%) are formed by the H-abstraction mechanism and only ~0.5% are produced via the insertion channel by the decomposition of $HC-CH_3$. Again, as in the case of the lower excess internal energy, the H-elimination rate from $HC-CH_3$, $k_4 = 9.75 \times 10^{12}$ s^{-1}, is much faster than the hydrogen-migration rate, $k_3 = 1.65 \times 10^{12}$ s^{-1}. This results in the fact that 88.4% of the $C_2H_3 + H$ products are formed from $HC-CH_3$ and only 11.6% are formed from the H_2C-CH_2 intermediate. One can also see that in this case the total removal rate of $HC-CH_3$ exceeds 10^{13} s^{-1}, indicating that the basic assumptions of the RRKM theory of a statistical distribution of the vibrational energy over all modes can break down, as redistribution of the internal energy occurs on the picosecond scale. Such high unimolecular rates can lead to non-RRKM (nonstatistical) behavior of the system.

A comparison of the $C_2H_3 + H$ and $CH + CH_3$ branching ratios at different excess internal energies indicates that the contribution of the $CH + CH_3$ products formed through the abstraction mechanism increases with the excess internal energy. This is related to the fact that the abstraction transition state TS2 is looser than the insertion transition state TS1 because the former has significantly lower vibrational frequencies than the latter (see Table 2). It is also worth noting that the reaction-path degeneracy for the abstraction process is twice as high as that for the insertion reaction via TS1 because the abstraction reaction can occur along two potential energy surfaces, $^3A'$ and $^3A''$, so that the electronic statistical weight for abstraction is twice as high as that for insertion. Although both the initial $C-CH_4$ complex and TS2 have C_{3v} symmetry and a ^3E electronic state, as mentioned in section 3.1, the reaction proceeds via C_s-symmetric configurations and therefore can follow two components of the ^3E PES, which are split along the reaction path. At excess internal energies higher than 2 eV, $CH + CH_3$ can eventually become the dominant reaction product. For instance, our calculations for the excess internal energy of 3 eV give the k_2/k_1 ratio as 2.22 (compared with 0.42 for 2 eV). Since the insertion mechanism nearly exclusively yields $C_2H_3 + H$ products (as is the case for the 2-eV excess internal energy), the $CH + CH_3$ and $C_2H_3 + H$ branching ratios can be reasonably well estimated on the basis of the k_2/k_1 ratio. Such an estimate for 3 eV gives the branching ratios of 68.9 and 31.1% for $CH + CH_3$ and $C_2H_3 + H$, respectively.

Moreover, at the excess internal energy of 4 eV, the CH + CH_3 branching ratio is expected to increase to 82.8%.

Until now, only the $C(^3P) + CH_4(^1A_1) \rightarrow CH(^2\Pi) + CH_3$ reaction channel has been recorded experimentally, through LIF measurements of the CH product.[9] Thus, there is an apparent disagreement between our theoretical results and experiment. This is most likely due to the fact that C_2H_3 + H, which are expected to be the major products at excess internal energies up to 2−2.5 eV, were not looked for in experiments, and spectroscopic measurements were targeted at the CH product only. Therefore, the formation of the vinyl radical and H atoms cannot be excluded on the basis of the available experimental evidence. New experimental measurements with detection of various possible reaction product pairs would be informative. Another question that needs to be clarified is the mechanism of CH formation in the reaction since our calculations predict that this product is formed almost exclusively by the abstraction mechanism, but Scholefield et al.[9] concluded that CH is produced via a carbene intermediate through the insertion mechanism. The statistical decomposition of the energized HC−CH_3 intermediate is very unlikely to lead to CH + CH_3 since this channel is 51.5 kcal/mol more endothermic (53.7 kcal/mol based on experimental heats of formation[30]) than the H loss producing C_2H_3 + H. Even though the variational transition states for the C−C bond cleavage in HC−CH_3 are looser than that for the H elimination, such a large energy difference is not likely to be overturned even at high excess internal energies. Hence, the experimental observation may be evidence of the nonstatistical decomposition of the carbene intermediate. Additional support for the possibility of nonstatistical behavior comes from the fact that at excess internal energies of 2 eV and higher the calculated unimolecular rates exceed 10^{13} s^{-1}, which is the limit of applicability of the RRKM theory.

3.4. Singlet−Triplet Intersystem Crossing. Using CASSCF-(10,10)/6−311(2+)G(2d,p) calculations, we were able to locate a minimum on the seam of crossing (MSX)[38] between the lowest singlet and triplet electronic states of C_2H_4. The MSX structure (see Figure 1) has C_s symmetry, and the crossing occurs between the $^1A'$ and $^3A''$ electronic states. The MSX geometry is rather similar to that of the triplet HC−CH_3 intermediate with slightly elongated C−C and C−H bonds, but the CCH angle at the CH group, 107.4°, is much smaller than that for the triplet optimized geometry, 132.2°. In this view, the geometry of MSX is closer to that of singlet HC−CH_3,[39] which has the corresponding CCH angle of 105.9°. Thus, the crossing can occur in a near vicinity of the HC−CH_3 intermediate. The energy of MSX computed at the CCSD(T)/6-311+G(3df,2p) level with the B3LYP/6-311G** ZPE is 61.1 kcal/mol lower than the energy of the reactants (i.e., it lies about 4 kcal/mol above the triplet HC−CH_3 structure). However, MSX is 0.7 kcal/mol higher in energy than the singlet HC−CH_3 structure.[39]

If the system undergoes intersystem crossing, then the reaction would proceed on the ground-state singlet PES of C_2H_4 and can be considered to be a decomposition of the energized ethylene molecule. According to experimental heats of formation,[30] the available energy for the singlet C_2H_4 fragmentation is 140.9 kcal/mol. This value is rather close to the energy of a 193-nm photon, 148.1 kcal/mol. Earlier,[39] we calculated the product branching ratio of ethylene photodissociation at 193 nm assuming rapid internal conversion into the ground electronic state and statistical dissociation on the ground-state PES. Our results gave the branching ratios for the H_2- and H-elimination channels as 73 and 27%. The C_2H_3 + H branching ratio was most likely somewhat underestimated because the possibility of H loss directly from the CH_3 group of the HC−CH_3 intermediate was not considered.[39] In any case, the $C_2H_2 + H_2$ channel contributes significantly to the reaction on the singlet PES, in a sharp contrast to the triplet-state C_2H_4 decomposition. Therefore, if the H_2 loss channel could be detected for the $C(^3P)$ + CH_4 reaction, this would be a clear indication that singlet−triplet intersystem crossing does occur along the reaction course. In a similar motif, recent crossed molecular beam studies of the $C(^3P) + C_2H_2$ reaction showed[4,40−42] that the spin-forbidden $C_3(^1\Sigma_g^+) + H_2$ product channel has a branching ratio of 30−40%, and this was attributed to facile singlet−triplet intersystem crossing for the C_3H_2 intermediate.[43]

4. Conclusions

The lowest triplet state PES of the $C(^3P) + CH_4$ reaction has been studied using the CCSD(T)/6-311+G(3df,2p)//QCISD/6-311G(d,p) method. Two reaction mechanisms have been found—H atom abstraction leading to the CH + CH_3 products and insertion of the carbon atom into methane's C−H bond leading to the triplet HC−CH_3 intermediate followed by its isomerization to triplet ethylene and/or decomposition through the elimination of a hydrogen atom. The insertion mechanism depicts a significantly lower barrier of 12.2 kcal/mol relative to the initial reactants as compared to the 26.9 kcal/mol barrier for the abstraction mechanism. The reactants can form a weak C−CH_4 complex bound by 0.8 kcal/mol. Molecular hydrogen elimination from the triplet HC−CH_3 and H_2C-CH_2 intermediates cannot occur, but the H_2 product could be formed in secondary C_2H_3 + H reactions producing triplet acetylene or vinylidene, which is not possible under single-collision conditions.

Microcanonical rate constants have been computed by employing the RRKM theory, and the fourth-order Runge−Kutta method was used to solve the system of kinetic equations. The numerical solutions that were obtained provide the concentrations of intermediates and products as functions of time, and the converged concentrations were utilized for calculations of product branching ratios. At the lower excess internal energy (12.2 kcal/mol), the reaction channels leading to CH + CH_3 are closed, and the exclusive reaction products are a vinyl radical plus a hydrogen atom. Ninety percent of the C_2H_3 + H products are formed through the fragmentation of HC−CH_3, and the rest (10%) are produced via the H_2C-CH_2 intermediate. At the higher excess internal energy (2 eV), CH + CH_3 can be formed either through H abstraction (the dominant channel) or through insertion and C−C bond cleavage in the HC−CH_3 intermediate (the minor channel). The calculated C_2H_3 + H and CH + CH_3 branching ratios at the excess internal energy of 2 eV are 69.8 and 30.2%, respectively. With further increases in the excess internal energy, the abstraction channel becomes more and more important because it has a significantly looser transition state than the insertion channel. As a result, the CH + CH_3 branching ratio increases to 68.9 and 82.8% at excess internal energies of 3 and 4 eV, respectively. Overall, the relative yields of the C_2H_3 + H and CH + CH_3 products are mainly governed by the ratio between the insertion and abstraction channels, as the former mostly leads to the atomic hydrogen loss and the latter results in CH + CH_3.

Singlet−triplet intersystem crossing is possible in the vicinity of the HC−CH_3 intermediate. If this crossing takes place and the reaction continues on the ground-state singlet PES, then the major products should be $C_2H_2 + H_2$ and C_2H_3 + H. Therefore, an observation of molecular hydrogen as the reaction product under single-collision conditions would indicate the feasibility

of the intersystem crossing. New experimental studies with the detection of various possible reaction product pairs are encouraged because they would be informative in further clarifying the reaction mechanism and dynamics.

Acknowledgment. This work was supported in part by Academia Sinica and the National Science Council of Taiwan, R.O.C. under grant NSC 91-2113-M-001-029 and by the Chinese Petroleum Research Fund. T.L.N is grateful to IAMS for a visiting fellowship.

References and Notes

(1) Mackay, C. In *Carbenes*; Moss, R. A., Jones, M., Eds.; Wiley: New York, 1975; Vol. 2.

(2) Shevlin, P. B. In *Reactive Intermediates*; Abramovich, R. A., Ed.; Plenum Publishing: New York, 1980; Vol. 1.

(3) Levine, R. D.; Bernstein, R. B. *Molecular Reaction Dynamics and Chemical Reactivity*; Oxford University Press: New York, 1987.

(4) Kaiser, R. I.; Mebel A. M. *Int. Rev. Phys. Chem.* **2002**, *21*, 307 and references therein.

(5) (a) Bruan, W.; Bass, A. M.; Davis, D. D.; Simmons, J. D. *Proc. R. Soc. London, Ser. A* **1969**, *312*, 417. (b) Husain, D.; Kirsch, L. J. *Trans. Faraday Soc.* **1971**, *67*, 2025. (c) Husain, D.; Young, A. N. *J. Chem. Soc., Faraday Trans. 2* **1975**, *71*, 525.

(6) Blint, R. J.; Newton, M. D. *Chem. Phys. Lett.* **1975**, *32*, 178.

(7) Skell, P. S.; Havel, J. J.; McGlinchey, M. J. *Acc. Chem. Res.* **1973**, *6*, 97.

(8) Scholefield, M. R.; Goyal, S.; Choi, J.-H.; Reisler, H. *J. Phys. Chem.* **1995**, *99*, 14605.

(9) Scholefield, M. R.; Choi, J.-H.; Goyal, S.; Reisler, H. *Chem. Phys. Lett.* **1998**, *288*, 487.

(10) Harding, L. B. *J. Phys. Chem.* **1983**, *87*, 441.

(11) Harding, L. B.; Guadagnini, R.; Schatz, G. C. *J. Phys. Chem.* **1993**, *97*, 5472.

(12) Scott, D. C.; de Juan, J.; Robie, D. C.; Schwartz-Lavi, D.; Reisler, H. *J. Phys. Chem.* **1992**, *96*, 2509.

(13) Guadagnini, R.; Schatz, G. C. *J. Phys. Chem.* **1996**, *100*, 18944.

(14) Ha, T.-K.; Nguyen, M. T.; Vanquickenborne, L. G. *Chem. Phys. Lett.* **1982**, *92*, 459.

(15) Gallo, M. M.; Schaefer, H. F., III. *J. Phys. Chem.* **1992**, *96*, 1515.

(16) Sakai, S.; Deisz, J.; Gordon, M. S. *J. Phys. Chem.* **1989**, 87, 1888.

(17) (a) Pople, J. A.; Head-Gordon, M.; Raghavachari, K. *J. Chem. Phys.* **1987**, *87*, 5968. (b) Gauss, J.; Cremer, D. *Chem. Phys. Lett.* **1988**, *150*, 280. (c) Salter, E. A.; Trucks, G. W.; Bartlett, R. J. *J. Chem. Phys.* **1989**, *90*, 1752. (d) Lee, T. J.; Taylor, P. R. *Int. J. Quantum Chem., Symp.* **1989**, *23*, 199. (e) Lee, T. J.; Rendell, A. P.; Taylor, P. R. *J. Phys. Chem.* **1990**, *94*, 5463.

(18) (a) Purvis, G. D.; Bartlett, R. J. *J. Chem. Phys.* **1982**, *76*, 1910. (b) Scuseria, G. E.; Janssen, C. L.; Schaefer, H. F. III. *J. Chem. Phys.* **1988**, *89*, 7382. (c) Scuseria, G. E.; Schaefer, H. F., III. *J. Chem. Phys.* **1989**, *90*, 3700. Pople, J. A.; Head-Gordon, M.; Raghavachari, K. *J. Chem. Phys.* **1987**, *87*, 5968.

(19) Hehre, W. J.; Radom, L.; Schleyer, P. v. R.; Pople, J. A. *Ab Initio Molecular Orbital Theory*; Wiley: New York, 1986.

(20) (a) Becke, A. D. *J. Chem. Phys.* **1993**, *98*, 5648. (b) Lee, C.; Yang, W.; Parr, R. G. *Phys. Rev. B* **1988**, *37*, 785.

(21) (a) Werner, H.-J.; Knowles, P. J. *J. Chem. Phys.* **1985**, *82*, 5053. (b) Knowles, P. J.; Werner, H.-J. *Chem. Phys. Lett.* **1985**, *115*, 259.

(22) (a) Werner, H.-J.; Knowles, P. J. *J. Chem. Phys.* **1988**, *89*, 5803. (b) Knowles, P. J.; Werner, H.-J. *Chem. Phys. Lett.* **1988**, *145*, 514.

(23) Dunning, T. H., Jr. *J. Chem. Phys.* **1989**, *90*, 1007.

(24) MOLPRO is a package of ab initio programs written by H.-J. Werner and P. J. Knowles with contributions from J. Almlöf, R. D. Amos, M. J. O. Deegan, S. T. Elbert, C. Hampel, W. Meyer, K. Peterson, R. Pitzer, A. J. Stone, P. R. Taylor, and R. Lindh.

(25) Frisch, M. J.; Trucks, G. W.; Schlegel, H. B.; Scuseria, G. E.; Robb, M. A.; Cheeseman, J. R.; Zakrzewski, V. G.; Montgomery, J. A., Jr.; Stratmann, R. E.; Burant, J. C.; Dapprich, S.; Millam, J. M.; Daniels, A. D.; Kudin, K. N.; Strain, M. C.; Farkas, O.; Tomasi, J.; Barone, V.; Cossi, M.; Cammi, R.; Mennucci, B.; Pomelli, C.; Adamo, C.; Clifford, S.; Ochterski, J.; Petersson, G. A.; Ayala, P. Y.; Cui, Q.; Morokuma, K.; Malick, D. K.; Rabuck, A. D.; Raghavachari, K.; Foresman, J. B.; Cioslowski, J.; Ortiz, J. V.; Stefanov, B. B.; Liu, G.; Liashenko, A.; Piskorz, P.; Komaromi, I.; Gomperts, R.; Martin, R. L.; Fox, D. J.; Keith, T.; Al-Laham, M. A.; Peng, C. Y.; Nanayakkara, A.; Gonzalez, C.; Challacombe, M.; Gill, P. M. W.; Johnson, B. G.; Chen, W.; Wong, M. W.; Andres, J. L.; Head-Gordon, M.; Replogle, E. S.; Pople, J. A. *Gaussian 98*, revision A.7; Gaussian, Inc.: Pittsburgh, PA, 1998.

(26) Eyring, H.; Lin, S. H.; Lin, S. M. *Basic Chemical Kinetics*; Wiley: New York, 1980.

(27) Robinson, P. J.; Holbrook, K. A. *Unimolecular Reactions*; Wiley: New York, 1972.

(28) Steinfeld, J. I.; Francisco, J. S.; Hase, W. L. *Chemical Kinetics and Dynamics*; Prentice Hall: Englewood Cliffs, NJ, 1999.

(29) Scott, A. P.; Radom, L. *J. Phys. Chem.* **1996**, *100*, 16502.

(30) *NIST Chemistry Webbook*; NIST Standard Reference Database Number 69, February 2000 Release (http://webbook.nist.gov/chemistry/).

(31) Gonzalez, C.; Schlegel, H. B. *J. Phys. Chem.* **1990**, *94*, 5523.

(32) Bach, R. D.; Su, M.-D.; Aldabbagh, E.; Andres, J. L.; Schlegel, H. B. *J. Am. Chem. Soc.* **1993**, *115*, 10237.

(33) Mebel, A. M.; Morokuma, K.; Lin, M. C. *J. Chem. Phys.* **1995**, *103*, 3440.

(34) Kurosaki, Y.; Takayanagi, T. *J. Chem. Phys.* **2000**, *113*, 4060.

(35) Le, T. N.; Mebel, A. M.; Kaiser, R. I. *J. Comput. Chem.* **2001**, *22*, 1522.

(36) Lin, S. H.; Lau, K. H.; Eyring, H. *J. Chem. Phys.* **1971**, *55*, 5657.

(37) Morokuma, K.; Eu, B. C.; Karplus, M. *J. Chem. Phys.* **1969**, *51*, 5193.

(38) The computer program for the MSX search was written by Q. Cui, K. Dunn, and K. Morokuma. Some details of the algorithm have been described in Dunn, K.; Morokuma, K. *J. Chem. Phys.* **1995**, *102*, 4904 and Cui, Q. Ph.D. Thesis, Emory University, Atlanta, GA, 1998. The program uses the HONDA 8.4 package by M. Dupuis.

(39) (a) Chang, A. H. H.; Mebel, A. M.; Yang, X.-M.; Lin, S. H.; Lee, Y. T. *Chem. Phys. Lett.* **1998**, *287*, 301. (b) Chang, A. H. H.; Mebel, A. M.; Yang, X.-M.; Lin, S. H.; Lee, Y. T. *J. Chem. Phys.* **1998**, *109*, 2748.

(40) Kaiser, R. I.; Le, T. N.; Nguyen, T. L.; Mebel, A. M.; Balucani, N.; Lee, Y. T.; Stahl, F.; Schleyer, P. v. R.; Schaefer, H. F., III. *Faraday Discuss.* **2001,** *119*, 51.

(41) Casavecchia, P.; Balucani, N.; Cartechini, L.; Capozza, G.; Bergeat, A.; Volpi, G. G. *Faraday Discuss.* **2001**, *119*, 27.

(42) Cartechini, L.; Bergeat, A.; Capozza, G.; Casavecchia, P.; Volpi, G. G. *J. Chem. Phys.* **2002**, *116***,** 5603.

(43) Mebel, A. M.; Jackson, W. M.; Chang, A. H. H.; Lin, S. H. *J. Am. Chem. Soc.* **1998**, *120*, 5751.